Experimental evidence for predicted magnetotransport anomalies in rectangular superlattices

M. C. Geisler,[1] S. Chowdhury,[1,*] J. H. Smet,[1] L. Höppel,[1] V. Umansky,[2] R. R. Gerhardts,[1] and K. von Klitzing[1]
[1]*Max-Planck-Institut für Festkörperforschung, Heisenbergstrasse 1, D-70569 Stuttgart, Germany*
[2]*Braun Center for Submicron Research, Weizmann Institute of Science, Rehovot 76100, Israel*
(Received 23 December 2004; revised manuscript received 15 March 2005; published 12 July 2005)

We investigate commensurability oscillations in the magnetoresistances of unstressed ungated rectangular two-dimensional superlattices of different periods. The amplitude of the commensurability oscillations in these systems exhibits a nonmonotonic dependence on the applied magnetic field, which is not present in 1D or square superlattices. Furthermore, the high and low resistance directions switch between the two axial directions of the superlattices depending on the magnetic field. Our observations are explained by the drift of the cyclotron motion guiding center along contours of a magnetic-field-dependent effective potential as put forward in a recent theory. Comparison of the data with the theoretical predictions shows good agreement. For a larger modulation amplitude, we observe a flattening of commensurability oscillation minima, which is also predicted by the calculation.

DOI: 10.1103/PhysRevB.72.045320 PACS number(s): 72.20.My, 73.40.Kp, 73.50.Jt

I. INTRODUCTION

Magnetotransport in two-dimensional electron systems (2DESs), subjected to the periodic potential of a one-dimensional or two-dimensional superlattice and a perpendicular magnetic field B, exhibits several interesting commensurability effects, which have fascinated many researchers over the last four decades. Some of the effects are of pure quantum mechanical origin, others—like certain types of commensurability or "Weiss" oscillations (COs)—were first considered as quantum effects, but have later also been explained semiclassically. In the present work we will investigate transport in samples with rectangular superlattices, which can well be described by a simple harmonic modulation potential of the form

$$V(x,y) = V_x \cos(2\pi x/a) + V_y \cos(2\pi y/b), \qquad (1)$$

with periods $a \neq b$ and comparable amplitudes V_x and V_y. For such superlattices a recent semiclassical calculation[1] has predicted an intriguing nonmonotonic dependence of the CO amplitudes on the applied magnetic field, which is neither known for 1D nor for square superlattices, and has so far neither been confirmed by quantum calculations nor by experiments.

COs were first discovered in high-mobility GaAs-(AlGa)As heterostructures with holographically defined 1D superlattices,[2] and were explained quantum mechanically: the periodic potential lifts the macroscopic degeneracy of the Landau levels and leads to eigenstates, which, in contrast to the unperturbed Landau states, carry current and form "Landau bands" with a B-dependent, oscillatory width, shrinking to zero at equidistant $1/B$ values. These eigenstates give rise to an oscillatory "band conductivity" contribution,[3–6] which adds to the usual "scattering conductivity." The latter describes the electron transport in the direction of the applied electric field as the result of scattering processes. Since it is proportional to the square of the density of states,[7] the scattering conductivity will produce COs with maxima when the Landau bands become flat and the band conductivity vanishes.[5,6] Thus, the COs of scattering and band conductivities will have opposite phases. Both types of COs have been observed in the early experiments.[2,3] Very soon it was pointed out[8] that the COs of the band conductivity, in contrast to those of the scattering conductivity, can also be understood in semiclassical terms as the result of a guiding center drift of the classical cyclotron orbits of electrons at the Fermi energy (considering the 2DES as a degenerate Fermi gas).

Extension of the pioneering experiment by Weiss *et al.*[2] to 2D superlattices showed COs of much smaller amplitudes than those observed in the *band conductivity* for the corresponding 1D modulations, but comparable in amplitude and phase with the *scattering conductivity* observed in the 1D modulation case.[9] This apparent suppression of the band conductivity in 2D superlattices was again interpreted quantum mechanically.[9,10] For a 2D superlattice and p/q flux quanta per unit cell, the quantum calculation yields a splitting of the LLs into p subbands which are q-fold degenerate (essentially the Hofstadter spectrum).[11–13] If collision broadening effects are so weak that spectral functions of different subbands have little overlap, the calculated band conductivity is considerably suppressed as compared to that calculated for the corresponding situation with a 1D modulation. This suppression becomes more effective with increasing strength of the 2D modulation and with increasing mobility.[9,10] This is, of course, a rather subtle argument, since the subband splitting was not observed in the experiments under consideration. Direct observation of the subband splitting in higher LLs and its consequences for the integer-quantized Hall effect[14,15] requires very low temperature and samples with very high mobility.[16,17]

The application of the guiding center picture to commensurability effects in 2D superlattices was first restricted to a perturbative calculation for small amplitudes of the modulation potential, which was assumed to be additive, $V(x,y) = V_x(x) + V_y(y)$.[18,19] In this approximation, just as in an equivalent perturbative solution of Boltzmann's equation, the modulation effects in x and y direction decouple, and no

suppression of the COs is obtained.[20] Numerical solution of the full Boltzmann equation without such a weak-potential approximation, on the other hand, yields a drastic suppression of the COs for large modulation amplitude and high mobility.[20] The interest in the guiding center drift model was revived by work of Grant *et al.*[21] and of Chowdhury *et al.*,[22] who emphasized that, in superlattices with rectangular symmetry, part of the guiding centers drift along pinned closed orbits and thus should not contribute to the band conductivity, i.e., should lead to a suppression of the COs. In subsequent work by Gerhardts and Zwerschke,[1] the guiding center drift model was used for a detailed calculation of COs and their suppression in rectangular symmetries. For intermediate magnetic field strengths and not too strong modulations, the results obtained in Ref. 20 by numerical solution of the full Boltzmann equation (which requires heavy numerical work and large computation time) could be reproduced. A direct comparison of the predictions made in Ref. 1 with quantum calculations or experimental results is, however, still missing. It is clear that the guiding center approach can only make sense if the cyclotron motion is more rapid than the guiding center drift, i.e., for strong enough B and for weak modulations.

Of special interest are the predictions of Ref. 1 for modulations with additive potentials in the x and the y direction, with different periods $a \neq b$ and comparable modulation strengths $V_x \sim V_y$. In such a 2D superlattice the guiding centers should move along the equipotential lines of an effective potential with the same periods a and b, but with effective modulation strengths $V_x^{\mathrm{eff}}(B)$ and $V_y^{\mathrm{eff}}(B)$. The oscillatory B-dependencies of $V_x^{\mathrm{eff}}(B)$ and $V_y^{\mathrm{eff}}(B)$ are different,[1] due to the different periods $a \neq b$ (see Sec. III B below). Then, sweeping the magnetic field, one should find situations with $V_x^{\mathrm{eff}}(B)=0$, in which the guiding centers can only move along open orbits in x direction, situations with $V_y^{\mathrm{eff}}(B)=0$, with only open orbits in y direction, and situations with $V_x^{\mathrm{eff}}(B)=V_y^{\mathrm{eff}}(B)$, with only closed orbits for the guiding centers. Thus, sweeping B should cover situations with effectively 1D modulations in y or x direction and also situations with a strong suppression of the guiding center contribution to the conductivities.

The aim of the present work was to fabricate such rectangular superlattices on a series of samples and to measure the commensurability oscillations in ρ_{xx} and ρ_{yy}, in order to check the predictions of Ref. 1. To obtain sufficiently different periods with still comparable modulation strengths in both directions, we investigated unstressed ungated heterostructures with etched superlattices of different periods having the ratio $a:b \approx 1.3$ in each case. We, indeed, observe essentially all the predicted behavior in our data: a nonmonotonic decay of the CO amplitudes with decreasing magnetic field, a magnetic-field-dependent interchange of high and low resistivity directions of the rectangular superlattice, and indications for a flattening of the CO minima for relatively high mobility or modulation amplitudes.

II. SAMPLE PREPARATION AND MEASUREMENT PROCEDURES

This work was carried out on two different GaAs-AlGaAs heterostructures grown on (100) GaAs substrates. The heterostructures contained a 2DES 42.5 nm below the surface. Hall bars with L-shaped mesas [see Fig. 1(a)] were fabricated with standard lithographic techniques. They were 20 μm wide and the geometry factor (the ratio of the distance between the voltage contacts and the sample width) was equal to 1. When unmodulated, the 2DES of the first heterostructure (A) showed a carrier density of $n=3.2\times10^{15}$ m^{-2} and a transport mobility $\mu=80$ m^2 V^{-1} s^{-1} at 4 K. After a brief illumination with a light emitting diode at 4 K, the mobility improved to 100 m^2 V^{-1} s^{-1} for a carrier density of 5×10^{15} m^{-2}. In the second heterostructure (B), these quantities were $n=3\times10^{15}$ m^{-2} and $\mu=83$ m^2 V^{-1} s^{-1} without illumination and $n=4\times10^{15}$ m^{-2} and $\mu=130$ m^2 V^{-1} s^{-1} after illumination.

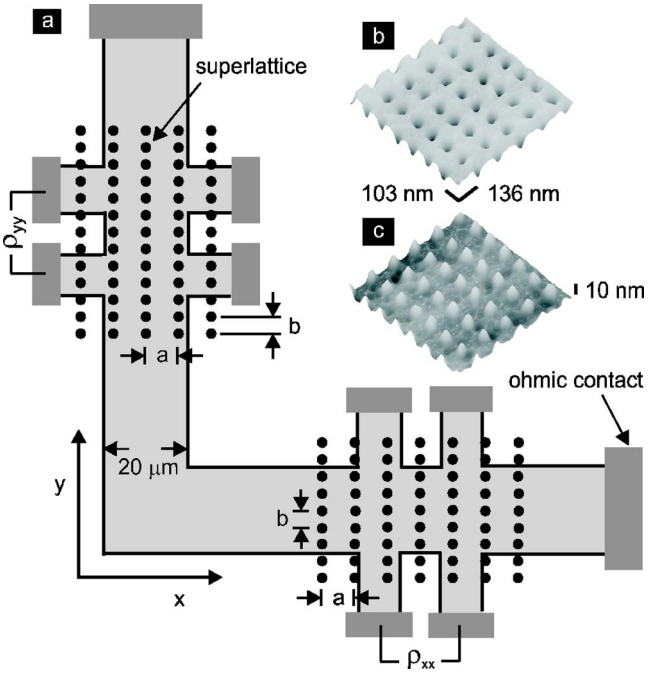

FIG. 1. (a) Sketch of the L-shaped Hall bar geometry showing the extent and orientation of the superlattices. The x- and y-directions coincide with the cleavage directions of the (100) GaAs wafer. (b) Normal and (c) inverted views of a representative AFM measurement on an etched 136 nm $\times$ 103 nm period superlattice after removal of the resist.

Patterns of about 50 nm diameter holes arranged on a rectangular superlattice were produced with high resolution electron beam lithography in a 90 nm thick PMMA resist layer coating the Hall bar. All rectangular lattices had the same ratio $a:b \approx 1.3$ of lattice constants a and b in the two perpendicular directions. The main axes of the lattices were oriented along and across the Hall bar, i.e. the cleavage directions of the (100) GaAs substrate [see Fig. 1(a)]. The area of each superlattice was large enough to cover more than an entire active area on the Hall bar, as depicted in Fig. 1(a). A room-temperature shallow wet etching process transferred the pattern to the heterostructure material: First, the oxide on the sample surface was removed by a 15 s etch in 40 ml deionized water with 10 ml concentrated hydrochloric acid and one drop of the surfactant benzalkonium chloride. The

surfactant is reducing the surface tension of the used etchants which in turn become able to reach into the nanoscale holes in the PMMA. As etch stop the sample was dipped into isopropyl alcohol for 60 s and blown dry in a N_2 flow. To transfer the electron beam pattern, the sample was subsequently etched in 10 ml citric acid solution (prepared by mixing 10 g citric acid monohydrate powder and 10 g deionized water), 30 ml 30% hydrogen peroxide and one drop of surfactant. By changing the etch time from 15 s to 60 s, the etch depth and the resulting modulation strength were adjusted. Finally, the sample was rinsed 30 s in 50 ml deionized water with a drop of surfactant to stop the etching, further rinsed in flowing deionized water for 60 s and blown dry with N_2. The resist was then entirely removed. In AFM studies, the depth of the holes etched at the surface of the Hall bars was found to be about 10 nm. Figures 1(b) and 1(c) display normal and inverted AFM images of the etched superlattice after the removal of the resist. No gate is deposited to avoid stress.

The magnetoresistances of the devices were measured using standard lock-in techniques at 4 K after a brief illumination. The mobility is reduced by the etching process to $\mu \approx 55\ \mathrm{m^2\,V^{-1}\,s^{-1}}$ at an electron density of $n=4.4\times10^{15}\ \mathrm{m^{-2}}$ for heterostructure (A) and $\mu \approx 65\ \mathrm{m^2\,V^{-1}\,s^{-1}}$ at $n=4.3\times10^{15}\ \mathrm{m^{-2}}$ for heterostructure (B). To simultaneously acquire the ρ_{xx} and ρ_{yy}-magnetoresistances for transport in the two orthogonal directions of the rectangular superlattice, two nominally identical superlattices oriented in the same direction with respect to the crystal directions were produced on the two arms of the L-shaped Hall bar [see Fig. 1(a) in which x and y are the cleavage directions]. Both superlattices are etched at the same time, and therefore we assume that the modulation strengths are similar for both.

The source of modulation has been identified as originating solely from the depletion effect. To this end, we studied square superlattices of 100 nm period. At the etched holes, the surface states are closer to the dopants. Hence a density modulation is introduced at the 2DES.[23] Combination of this depletion effect and stress modulation is known to introduce asymmetry between the two cleavage directions on (100) GaAs substrates in the case of square superlattices.[22,24] However, here no asymmetry was observed between the COs for transport along the x- and y-directions. In view of the absence of asymmetry, we conclude that the modulation is exclusively due to the depletion effect.

III. KEY EXPERIMENTAL OBSERVATIONS

A. Resistance traces

Figure 2 shows the magnetoresistances measured at 4 K for transport along the two axial directions of a rectangular superlattice with lithographic periodicities of $a=136$ nm along the $[01\bar{1}]$ direction and $b=103$ nm along the [011] direction of the GaAs crystal ($a:b\approx1.3$). The x-direction is taken along the longer period and the y-direction along the shorter period of the modulation. The minima of the COs in the trace for transport along the 136 nm period occur when $2R_c=(k_a-1/4)a$, where R_c is the cyclotron radius and $k_a=1,2,3,\ldots$, while those in the trace for transport along the 103 nm period coincide with the condition $2R_c=(k_b-1/4)b$ where $k_b=1,2,3,\ldots$. Hence, the location of the minima is identical to those anticipated for a 1D modulated system with period a and b respectively.[3] Unique to 2D superlattices of rectangular shape are the following three striking features of the data:

(1) The amplitude of the CO peaks do not monotonically decrease as in 1D-modulated systems. For transport along the longer period (136 nm), i.e. in ρ_{xx}, the CO peak between the $k_a=3$ and 4 minima is significantly suppressed in amplitude (for instance as compared with its neighboring peak at lower magnetic field, i.e. the CO peak between the $k_a=4$ and 5 minima).

(2) Similarly, for transport along the shorter period (103 nm), i.e. in ρ_{yy}, the CO peak between the $k_b=6$ and 7 minima is significantly enhanced in amplitude (compared with its neighboring peak at higher magnetic field, i.e. the CO peak between the $k_b=5$ and 6 minima).

(3) The large CO peaks between the $k_a=2$ and 3 minima and the $k_b=2$ and 3 minima occur when the magnetoresistance in the other axial direction exhibits a broad CO minimum. This corresponds to an interchange of the high and low resistance directions between the two axial directions of the superlattice.

These three characteristics of the COs in rectangular lattices will be referred to as *suppression, enhancement*, and *switching*.

B. Adjusting the modulation potential

All of these features have been predicted by the theory outlined in Ref. 1. The underlying physical picture is the following. According to Refs. 21 and 1, the instantaneous velocity of the guiding center, averaged over a perimeter of the unperturbed cyclotron orbit, is given by[18]

$$\boldsymbol{v}_{\mathrm{avg}} = -\,\boldsymbol{\nabla} V^{\mathrm{eff}} \times \boldsymbol{B}/B^2, \tag{2}$$

where V^{eff} is an effective potential. Hence the guiding center drifts along the contours of the effective potential. Considering only the fundamental Fourier components, which will prove to be sufficient in the following, we can write the actual potential modulation in the rectangular superlattice in the form of Eq. (1). The corresponding effective potential is given by[18]

$$V^{\mathrm{eff}}(X,Y) = V_x^{\mathrm{eff}} \cos(2\pi X/a) + V_y^{\mathrm{eff}} \cos(2\pi Y/b), \tag{3}$$

where

$$V_x^{\mathrm{eff}} = V_x J_0(2\pi R_c/a), \quad V_y^{\mathrm{eff}} = V_y J_0(2\pi R_c/b). \tag{4}$$

Here (x,y) refer to the coordinates of the electron and (X,Y) to those of the guiding center of the cyclotron orbit. J_0 is the Bessel function of the first kind. As before, the x-direction is taken to be along the longer axial lattice constant a and the y-direction along the shorter axial lattice constant b.

A study of the behavior of this effective potential turns out particularly instrumental. The most notable property of the effective potential in the current context is that the magnetic field dependencies of V_x^{eff} and V_y^{eff} are different, as the

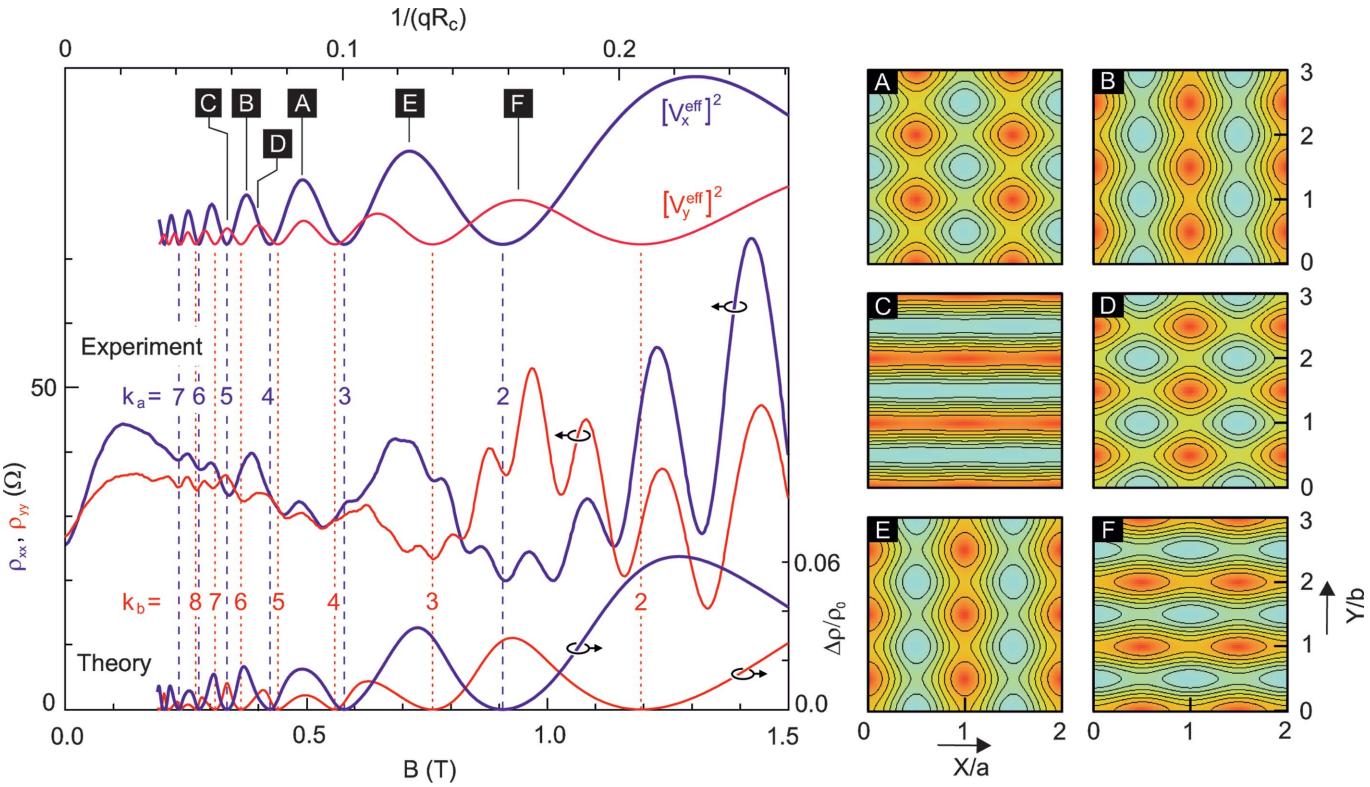

FIG. 2. (Color) Left panel, middle: Magnetoresistances measured at 4 K for transport along the 136 nm (x-direction, thick blue) and the 103 nm (y-direction, thin red) period directions of a rectangular superlattice. Bottom: Magnetoresistances ρ_{xx} (blue) and ρ_{yy} (red) calculated using Ref. 1 for the parameters $V_x=5.6\%\ E_F$, $V_y=3.9\%\ E_F$, a ratio $a:b=1.32$ and $q\lambda=26$. The vertical lines indicate the calculated B values of the CO minima of ρ_{xx} for indices k_a (blue dashed) and of ρ_{yy} for indices k_b (red dotted). They coincide with the zeroes of the corresponding effective potential amplitudes $[V_x^{\text{eff}}]^2$ (blue line) and $[V_y^{\text{eff}}]^2$ (red line) shown, in arbitrary units, at the top as function of $1/(qR_c)$. Right panels: A, B, C, D, E, and F show the contours of the effective potential $V_x^{\text{eff}}\cos(2\pi X/a)+V_y^{\text{eff}}\cos(2\pi Y/b)$ at the peaks marked in the left graph by A, B, C, D, E, and F, respectively. The contours in these panels correspond to guiding center trajectories in real space.

arguments of the two Bessel functions involve the different periodicities a and b. The Bessel functions entering the X- and Y-dependent components of the effective potential are identical to those Bessel functions describing the transport in 1D modulated systems along the direction of modulation.[4,5,8] The zeroes of these Bessel functions coincide with the CO-minima. Hence, in a 2D modulated system with periods a and b the CO-minima agree exactly with those of the corresponding 1D systems at the zeroes of $[V_x^{\text{eff}}]^2$ and $[V_y^{\text{eff}}]^2$. For large arguments of the Bessel functions, these zeros occur in excellent approximation when $2R_c=(k_a-1/4)a$ and $2R_c=(k_b-1/4)b$ where $k_a,k_b=1,2,3,\ldots$. Figure 2 depicts the B-dependence of $[V_x^{\text{eff}}]^2$ and $[V_y^{\text{eff}}]^2$ (uppermost traces, arbitrary units) for $a=136$ nm and $b=103$ nm, calculated for $V_x/V_y=1.45$. The carrier density 4.4×10^{15} m^{-2}, which determines R_c, is obtained from the Shubnikov-de Haas (SdH) oscillations. Whereas the peak values in the traces of $|V_x^{\text{eff}}|^2$ and $|V_y^{\text{eff}}|^2$ decrease monotonically with decreasing magnetic field, the peak values of the COs in the experimental traces apparently do not. To understand this, we calculated $\rho_{xx}(B)$ and $\rho_{yy}(B)$ for the same parameter values from the model of Ref. 1 and plotted the results near the bottom of Fig. 2. The ratio $V_x/V_y=1.45$ is chosen in order to obtain for the theoretical resistance traces an overall appearance similar to the corresponding experimental traces (of course apart from the SdH oscillations, which are not included in the calculation). Other values in the range $1.3\lesssim V_x/V_y\lesssim1.7$ would also be acceptable and compatible with the two following estimates:

At present, no theoretical calculation on 2D superlattices is available to directly extract the potential modulation amplitudes from the magnitude of the COs. Referring back to Fig. 2, one can see that for some of the CO peaks, e.g., the one at C in ρ_{yy}, the effective potential is close to 1D. Although this quasi-one-dimensionality refers only to the effective potential, we evaluate the COs at these positions using an analytic form of the magnetic field dependence of the COs for 1D superlattices proposed by Mirlin and Wölfle.[25] Taking the heights $\Delta\rho$ of the CO peaks at B and C and a total (quantum) scattering time $\tau_0\approx1.5$ ps, we obtain from Eq. (49) in Ref. 25 the potential modulation amplitudes $V_x=5.9\%\ E_F$ and $V_y=3.5\%\ E_F$, with $V_x/V_y=1.7$. In 1D superlattices the modulation amplitude can be estimated from the saturation field B_0 of the positive magnetoresistance at low magnetic fields.[26] Extending this estimate naively to our case of a 2D superlattice, we find for the data of Fig. 2 $V_x=4.8\%\ E_F$ and $V_y=3.8\%\ E_F$, with $V_x/V_y\approx1.3$. Since both estimates yield modulation amplitudes of the same order of magnitude, we believe that our choice of model parameters

is reasonable for a qualitative understanding of the experimental results.

At the zeros of the Bessel functions, the effective potential amplitudes $[V_x^{\mathrm{eff}}]^2$ and $[V_y^{\mathrm{eff}}]^2$ drop to zero and these zeroes indeed align with the minima of the COs observed in ρ_{xx} and ρ_{yy}. The phases of the squared effective potential amplitudes, plotted as functions of B near the top of Fig. 2, are essentially the same as those of ρ_{xx} and ρ_{yy}, respectively. As is evident from the plot, the dominance of $|V_x^{\mathrm{eff}}|$ over $|V_y^{\mathrm{eff}}|$ changes as a function of the magnetic field. The ratio $\alpha=|V_x^{\mathrm{eff}}|/|V_y^{\mathrm{eff}}|$ is the key to understanding the various features of the COs in question (suppression, enhancement, and switching) as it controls the shape of the effective potential, i.e. the distribution of open and closed contours as well as the direction along which open contours run. Since these contours are the trajectories of the guiding centers in real space, many open contours in a particular direction implies an enhancement of the conductivity in this direction or, equivalently, an increase of the resistivity in the perpendicular direction.

IV. DETAILED COMPARISON WITH THEORY

A. Suppression

In contrast to the peak values of the $|V_x^{\mathrm{eff}}|^2$- and $|V_y^{\mathrm{eff}}|^2$-traces in the upper part of Fig. 2, the peak values of the measured COs show a nonmonotonic dependence on the magnetic field. For instance, the CO peak in ρ_{xx} (blue curve) between the $k_a=3$ and 4 minima at the magnetic field position with the label A is much lower than the neighboring peaks at the field values with labels B and E. A similar reduction of the peak height at A is seen in the corresponding theoretical curve for ρ_{xx} at the bottom of Fig. 2. The explanation goes as follows: Near A both the $|V_x^{\mathrm{eff}}|^2$ and the $|V_y^{\mathrm{eff}}|^2$ traces have local maxima and the deviation of the ratio α from 1 is not so large as near B and E, where $|V_x^{\mathrm{eff}}|^2$ has local maxima while $|V_y^{\mathrm{eff}}|^2$ is close to local minima. As a consequence, in the cases B and E the effective modulation in x direction is much stronger than in y direction, with many open guiding center trajectories in y direction. This results in large, quasi-1D CO peaks in ρ_{xx}. At A, on the other hand, the effective potential has 2D character with more closed equipotentials and the CO peak is suppressed as compared with the 1D case. The contour plots of Figs. 2(A), 2(B), and 2(E), which have been calculated for $|V_y^{\mathrm{eff}}|=0.60|V_x^{\mathrm{eff}}|$, $|V_y^{\mathrm{eff}}|=0.32|V_x^{\mathrm{eff}}|$, and $|V_y^{\mathrm{eff}}|=0.34|V_x^{\mathrm{eff}}|$, support this explanation.

Similar arguments apply to the CO peak in ρ_{yy} (middle red curve: experiment; bottom red curve: theory) at A, which is lower than that labeled D between the $k_b=5$ and 6 minima. At D we have $|V_x^{\mathrm{eff}}|=1.07|V_y^{\mathrm{eff}}|$, so that nearly all equipotentials are closed [see Fig. 2(D)] and the guiding center contributions to both ρ_{xx} and ρ_{yy} are suppressed below the corresponding 1D cases. At A, however, we have open trajectories in the y direction but not in the x direction, and, as a consequence, the guiding center contribution to ρ_{yy} is even smaller than that to ρ_{xx}, which is already suppressed compared with its neighboring peaks. This behavior is clearly seen in both the theoretical and the experimental results.

Another feature, that is evident in the theoretical curve for ρ_{yy} and less clear but visible also in the experimental curve, is the asymmetry of the CO peaks between $k_b=3$ and 4 and between $k_b=5$ and 6. As compared to the corresponding maxima of $|V_y^{\mathrm{eff}}|^2$ in the upper part of Fig. 2, the maxima of the theoretical magnetoresistance curve are shifted towards the regions with lower values of $|V_x^{\mathrm{eff}}|^2$, since the guiding center contribution to ρ_{yy} is stronger suppressed in field intervals with $|V_y^{\mathrm{eff}}|^2<|V_x^{\mathrm{eff}}|^2$ than in those with $|V_x^{\mathrm{eff}}|^2<|V_y^{\mathrm{eff}}|^2$.

B. Enhancement

The peak of $|V_y^{\mathrm{eff}}|^2$ marked as C in Fig. 2 corresponds to the CO peak in ρ_{yy} between the $k_b=6$ and 7 minima. At this field value $|V_x^{\mathrm{eff}}|^2$ nearly vanishes, $\alpha=0.05$. Figure 2(C) displays the guiding center trajectories for this CO peak. One sees only open trajectories which run along the x direction. This situation is very similar to a 1D modulation in y direction, with an 1D-like, unsuppressed peak of the guiding center contribution to ρ_{yy} and no guiding center contribution to ρ_{xx}. Compared with the adjacent peaks in ρ_{yy}, the peak at position C appears as enhanced. This effect is present in both the experimental and the theoretical ρ_{yy} traces.

C. Switching

So far we have compared CO peaks in the ρ_{xx} and the ρ_{yy} curves only with adjacent peaks in the same curve. It is however also interesting to compare the curves with each other.

From the experimental traces in Fig. 2 one gets the impression that, in general, the COs in ρ_{xx} are stronger than those in ρ_{yy}. We have adapted potential strengths in the upper part of the figure so that the theoretical curves near the bottom of Fig. 2 reproduce this impression. The effective potential $|V_x^{\mathrm{eff}}|$ associated with the longer axial lattice constant is dominant for most of the magnetic field values. Hence, at these magnetic fields, open trajectories of the guiding center exist *exclusively* along the shorter axial lattice constant (y-direction), and the guiding center contribution to ρ_{xx} is considerably larger than that to ρ_{yy}. The CO peaks for transport along the shorter axial lattice constant (ρ_{yy}) at these magnetic fields are, however, not entirely absent. As a consequence of the finite mean free path and modulation strength, a guiding center follows during its lifetime only a fraction of the trajectory and its velocity in x direction does not average to zero.

Near the magnetic field values labeled B and E and near $B=1.3$ T the dominance of the COs in ρ_{xx} is clearly seen. There are, however, also B regions where ρ_{yy} is larger than ρ_{xx}, e.g., near the positions labeled C and F. At these positions $|V_y^{\mathrm{eff}}|^2$ has local maxima while $|V_x^{\mathrm{eff}}|^2$ becomes very small, so that the equipotential patterns of the effective potential are governed by open trajectories in the x direction [see Figs. 2(C) and 2(F), which was calculated for $|V_x^{\mathrm{eff}}|=0.31|V_y^{\mathrm{eff}}|$].

As Figs. 2(E) and 2(F) show, the open trajectories in these two cases run along the two orthogonal directions: in the y-direction in the first case and in the x-direction in the second. This corresponds to a complete switching of the guiding

center drift direction between the two *axial* directions of the superlattice and an interchange of the high and low resistivity directions. All the features discussed so far are in nice agreement with the theoretical predictions.[1]

D. Limitations of the guiding center model

There are several features of the experimental magnetoresistance traces, which have no counterpart in the theoretical traces at the bottom of Fig. 2, obtained within the simple semiclassical guiding center approximation.[1] For instance to reproduce the pronounced SdH oscillations (observed for $B \geqslant 0.6$ T), one needs a quantum calculation based on a modulation-induced single-electron Landau band structure, in which the group velocity takes over the role of the classical guiding center drift velocity. The oscillatory width of Landau bands yields COs, which appear as a modulation of the envelope of the SdH oscillations.[5,10] The superposition of the SdH oscillations makes it difficult to extract the positions of the CO minima from the experimental curves. Moreover, near these minima, which we understand as band-conductivity minima, one expects maxima of the scattering conductivities, related to density of states maxima.[9,10] Therefore, near the resistance minima quantum effects may cause differences between the experimental traces and the theoretical traces in Fig. 2.

Also the pronounced positive magnetoresistance at very low magnetic fields and the overall decrease of the resistances in the region $0.1\ \mathrm{T} \lesssim B \lesssim 1.0$ T are beyond the scope of the guiding center approach of Ref. 1. They can be reproduced by classical calculations based on the full Boltzmann equation.[20,27] The positive magnetoresistance has been explained by the motion of electrons on channeled trajectories along minima of the modulation potential.[26,27] Even if the guiding center approach seems meaningful (i.e., in Fig. 2 for $B \gtrsim 0.2$ T), the calculation based on Eq. (2) is not always reliable. It has been pointed out in Ref. 1 that Eq. (2) does not correctly describe the guiding center motion if the effective potential (3) vanishes. At B-values close to the $k_b=4$ and 5 minima, the effective potentials $|V_x^{\mathrm{eff}}|$ and $|V_y^{\mathrm{eff}}|$ are both very small and the distance of the experimental resistivity minima is apparently considerably smaller than the separation between the minima in the theoretical curves. At present we do not know whether this discrepancy could be resolved within the semiclassical approach [e.g., by a more reliable treatment of the guiding center motion than on the basis of Eq. (2)], or whether it is due to the above-mentioned quantum effects.

Finally we remark that, with decreasing B, the COs of the experimental traces decay much faster than those of the theoretical traces. As we know from calculations for 1D superlattices[25,27,28] as well as for square superlattices,[20] this points towards predominant small-angle scattering caused by finite-range impurity potentials. This is also not included in the approach of Ref. 1.

In view of all these limitations of the simple guiding center approach, we cannot expect a quantitative agreement between the calculations of Ref. 1 and the measured magnetoresistivity curves. However, qualitatively all predictions (nonmonotonic decrease of CO amplitudes, suppression, enhancement, and switching) are confirmed in our experiments.

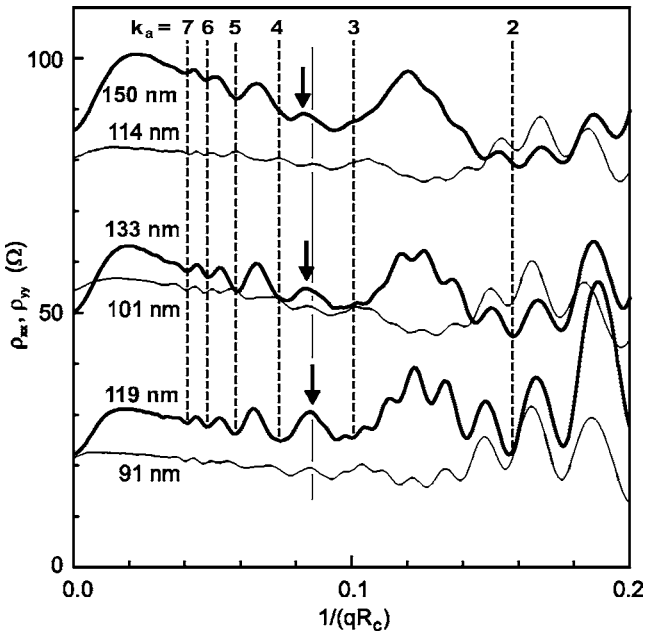

FIG. 3. Magnetoresistances measured at 4 K for transport in rectangular superlattices of three different pairs of lattice constants having the ratio 1.3: thick lines for transport along the longer periods (ρ_{xx}), thin lines for transport along the shorter periods (ρ_{yy}); periods are indicated. For clarity, the middle and the upper pair of traces have been offset by 30Ω and by 60Ω, respectively. The three CO minima (in ρ_{xx}) for $k_a=5$ occur at the same dashed vertical line. The CO peaks in ρ_{xx} between the $k_a=3$ and 4, indicated by downward arrows, are with increasing modulation period increasingly suppressed.

V. OTHER PERIODS AND MODULATION STRENGTHS

A. Scaling property

We have also compared the COs of rectangular superlattices for three different pairs of a- and b-values, while preserving the ratio $a:b \approx 1.3$. The superlattices are 150 nm × 114 nm, 133 nm × 101 nm, and 119 nm × 91 nm. The longer periods were along the [011] direction and the shorter periods were along the $[01\bar{1}]$ direction. The data are plotted in Fig. 3. The magnetic field axis is rescaled as $1/(qR_c)$, where $q=2\pi/\sqrt{ab}$, to take out both the density dependence and the dependence on period. Because $a:b$ is the same in each case, similar features can be seen at the same value of $1/(qR_c)$. The three CO minima for $k_a=5$ for instance occur at the same abscissa value in Fig. 3.

The important observation in Fig. 3 is related to the previously discussed suppressed CO peak between the $k_a=3$ and 4 minima. When comparing the traces obtained on the different superlattices, the suppression is found to be least effective in the case of the 119 nm period peak and most effective in the case of the 150 nm period peak. The superlattices were fabricated at the same time and hence the

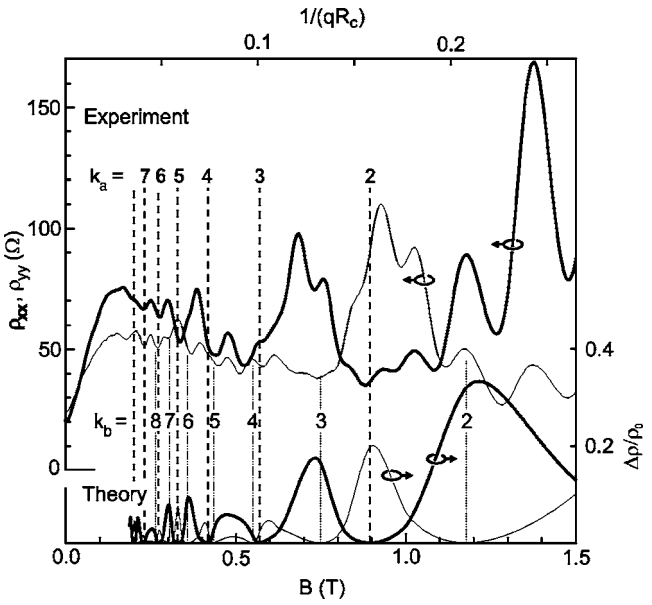

FIG. 4. (Top) Magnetoresistances measured at 4 K for transport along the 136 nm (thick line) and 103 nm (thin line) period of a rectangular superlattice on heterostructure B. The vertical lines mark the calculated magnetic field values of the CO minima for indices k_a and k_b. Note that the broad CO minima at $k_a=2$ and $k_b=3$ are flattened. Bottom: Magnetotransport calculation using Ref. 1 with $V_x=9\%\ E_F$, $V_y=7\%\ E_F$, the ratio $a:b=1.32$ and $q\lambda=37$.

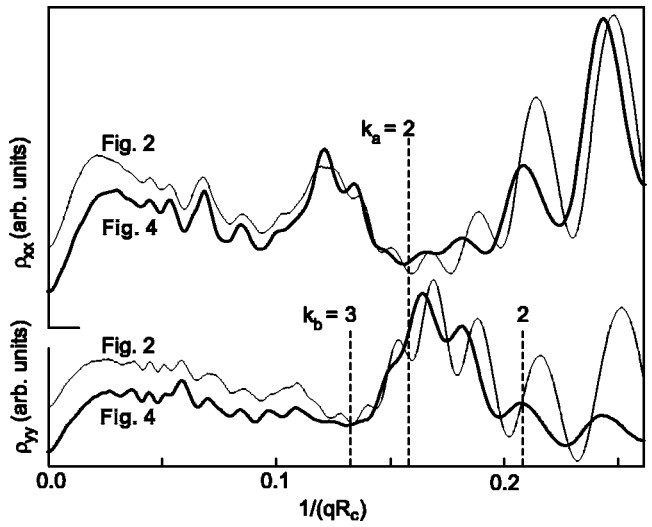

FIG. 5. The Magnetoresistances of Fig. 2 (thin) and Fig. 4 (thick) plotted versus $1/(qR_c)$, so CO minima are aligned. Note that the SdH oscillations for the CO minima at $k_a=2$ and $k_b=2,3$ are suppressed for the thick lines as compared to the thin lines.

depths of the etched holes are expected to be nearly the same in all cases. But the modulation amplitudes are expected to vary. Because of the exponential decay[18] with the distance of the 2DES from the heterostructure surface, a stronger modulation is associated with a larger period. The transport mobilities are essentially the same in all three cases. The data in Fig. 3 thus provide evidence of increasing suppression with increasing modulation at a given mobility. This is in agreement with the theory.[1] From Eq. (2), we conclude that the magnitude of the velocity of the guiding center drift is proportional to the gradient $|\nabla V^{\mathrm{eff}}|$. Therefore, this velocity increases with the modulation amplitude. Hence for a given mobility, if the velocity of the guiding centers is enhanced, more of them will be able to complete closed trajectories, which renders the suppression more effective. Of course, if the modulation is too large, then this picture will not hold as then one cannot average the drift velocity over the unperturbed cyclotron orbit to get the average velocity and Eq. (2) loses its validity.

B. Flattening of the commensurability minima

The data discussed so far were obtained from devices using heterostructure A. Devices from heterostructure B exhibited stronger modulations. Data for transport along the two axial directions of a 136 nm $\times$ 103 nm superlattice measured at 4 K after a brief illumination are depicted in Fig. 4. The 136 nm period was along the $[01\bar{1}]$ and the 103 nm period was along the [011] direction. As is evident, all the characteristics of the COs discussed in connection with the data of Fig. 2 are present in the data of Fig. 4. One additional feature in the data is a flattening and broadening of the CO minima in ρ_{xx} and ρ_{yy} at $k_a=2$ and $k_b=3$, respectively. This is best illustrated in Fig. 5, which is directly comparing the data of Fig. 2 (thin line) and Fig. 4 (thick line). For sample B (thick line), the SdH oscillations of ρ_{yy} are strongly suppressed near $1/(qR_c)\approx 0.13$, and at $1/(qR_c)\gtrsim 0.2$, and those of ρ_{xx} are suppressed near $1/(qR_c)=0.15$.

This magnetoresistance feature was predicted for relatively high mean free paths (e.g., for $q\lambda=800$ rather than 80; see Fig. 8 of Ref. 1), and we would expect it to be more pronounced, if we calculate λ from the transport time (this would yield $q\lambda\gtrsim 300$ for the data of Fig. 2). The large transport times in our samples result from the predominance of small-angle scattering, which was not considered in Ref. 1. Since already small changes of the momentum can lead to trajectories with very different guiding centers, we should calculate λ from the total scattering time τ_0 instead. This reduces the $q\lambda$ values by more than an order of magnitude, and we obtain $q\lambda\sim 26$ and ~ 37 for the data of Fig. 2 and Fig. 4, respectively. The modulation amplitudes are, however, much larger for the data of Fig. 4. Using the CO peaks between the $k_a=4$ and 5 minima and the $k_b=6$ and 7 minima, and the Mirlin and Wölfle[25] theory as described in Sec III B, the potential amplitudes are estimated to be $V_x=10\%\ E_F$ and $V_y=6\%\ E_F$ for the data of Fig. 4. Nevertheless, the magnetotransport calculation best reproduces the experimental data of Fig. 4 for a smaller ratio $V_x/V_y=1.3$ and amplitudes $V_x=9\%$ and $V_y=7\%$ of E_F. This is still nearly twice as large as the values for Fig. 2. According to Ref. 1, larger modulation and larger mean free path are complementary within the limits of the guiding center drift model. Hence, the larger modulation amplitudes enable the observation of this flattening of the CO minima in Fig. 4. This effect should be even more pronounced in samples with larger scattering times.

VI. CONCLUSIONS

In summary, we have investigated the COs in unstressed and ungated rectangular two-dimensional superlattices with a ratio of periods equal to 1.3. The characteristics of the observed COs can only be explained by the drift of the guiding center of the cyclotron motion along contours of a magnetic-field-dependent effective potential as envisaged in a recent magnetotransport theory.[1] For transport along the longer period, the CO peaks for which the asymmetry of the effective potentials is small were suppressed relative to their neighboring CO peaks at lower magnetic fields. In our systematic studies, the suppression was found to be more effective with increasing modulation amplitudes at a given transport mobility. For transport along the shorter periods, the CO peaks at which the effective potentials along the longer periods are small were enhanced relative to their neighboring CO peaks at higher magnetic fields. Magnetic-field-dependent switching of high and low resistance directions between the two axial directions of the superlattices was also observed. Comparison of the data with the theoretical calculation[1] showed good agreement. For a larger modulation amplitude, we observed a flattening of CO minima, which was predicted by the calculation.[1] None of these characteristic features can be explained by earlier perturbative calculations[18,19] which are valid for weak modulation only. In particular, the earlier semiclassical and quantum theories predict a monotonic decay of the CO amplitude with decreasing magnetic field which is not the case in the data. This puts forward the theoretical challenge of finding the quantum mechanical version of the semiclassical calculation.[1]

ACKNOWLEDGMENTS

We thank U. Waizmann, J. Meyer, M. Riek, and T. Reindl for technical assistance. We acknowledge financial support from the German Ministry of Science and Education and S.C. acknowledges support from the Alexander von Humboldt Foundation.

*Permanent address: Department of Physics, Shahjalal University of Science and Technology, Sylhet 3114, Bangladesh.

[1] R. R. Gerhardts and S. D. M. Zwerschke, Phys. Rev. B **64**, 115322 (2001).
[2] D. Weiss, K. von Klitzing, K. Ploog, and G. Weimann, Europhys. Lett. **8**, 179 (1989); see also in *High Magnetic Fields in Semiconductor Physics II*, Springer Series in Solid-State Sciences, edited by G. Landwehr (Springer-Verlag, Berlin, 1989), Vol. 87, p. 357.
[3] R. R. Gerhardts, D. Weiss, and K. v. Klitzing, Phys. Rev. Lett. **62**, 1173 (1989).
[4] R. W. Winkler, J. P. Kotthaus, and K. Ploog, Phys. Rev. Lett. **62**, 1177 (1989).
[5] C. Zhang and R. R. Gerhardts, Phys. Rev. B **41**, 12850 (1990).
[6] R. R. Gerhardts and C. Zhang, Phys. Rev. Lett. **64**, 1473 (1990); Surf. Sci. **229**, 92 (1990).
[7] T. Ando, A. B. Fowler, and F. Stern, Rev. Mod. Phys. **54**, 437 (1982).
[8] C. W. J. Beenakker, Phys. Rev. Lett. **62**, 2020 (1989).
[9] R. R. Gerhardts, D. Weiss, and U. Wulf, Phys. Rev. B **43**, R5192 (1991).
[10] D. Pfannkuche and R. R. Gerhardts, Phys. Rev. B **46**, 12606 (1992).
[11] M. Y. Azbel', Sov. Phys. JETP **19**, 634 (1964) [Zh. Eksp. Teor. Fiz. **46**, 929 (1964)].
[12] D. Langbein, Phys. Rev. **180**, 633 (1969).
[13] R. D. Hofstadter, Phys. Rev. B **14**, 2239 (1976).
[14] P. Středa, J. Phys. C **15**, L1299 (1982).
[15] D. J. Thouless, M. Kohmoto, M. P. Nightingale, and M. den Nijs, Phys. Rev. Lett. **49**, 405 (1982).
[16] C. Albrecht, J. H. Smet, K. von Klitzing, D. Weiss, V. Umansky, and H. Schweizer, Phys. Rev. Lett. **86**, 147 (2001).
[17] M. C. Geisler, J. H. Smet, V. Umansky, K. von Klitzing, B. Naundorf, R. Ketzmerick, and H. Schweizer, Phys. Rev. Lett. **92**, 256801 (2004).
[18] R. R. Gerhardts, Phys. Rev. B **45**, 3449 (1992).
[19] R. R. Gerhardts, Phys. Rev. B **53**, 11064 (1996).
[20] S. D. M. Zwerschke and R. R. Gerhardts, Physica B **298**, 353 (2001).
[21] D. E. Grant, A. R. Long, and J. H. Davies, Phys. Rev. B **61**, 13127 (2000).
[22] S. Chowdhury, C. J. Emeleus, B. Milton, E. Skuras, A. R. Long, J. H. Davies, G. Pennelli, and C. R. Stanley, Phys. Rev. B **62**, R4821 (2000).
[23] Y. Paltiel, D. Mahalu, H. Shtrikman, G. Bunin, and U. Meirav, Semicond. Sci. Technol. **12**, 987 (1997).
[24] S. Chowdhury, A. R. Long, E. Skuras, C. J. Emeleus, and J. H. Davies, J. Korean Phys. Soc. **39**, 529 (2001).
[25] A. D. Mirlin and P. Wölfle, Phys. Rev. B **58**, 12986 (1998).
[26] P. H. Beton, E. S. Alves, P. C. Main, L. Eaves, M. Dellow, M. Henini, O. H. Hughes, S. P. Beaumont, and C. D. W. Wilkinson, Phys. Rev. B **42**, 9229 (1990).
[27] R. Menne and R. R. Gerhardts, Phys. Rev. B **57**, 1707 (1998).
[28] J. Groß and R. R. Gerhardts, Phys. Rev. B **66**, 155321 (2002).